A&A 469, 309–317 (2007)
DOI: 10.1051/0004-6361:20066503

Astronomy & Astrophysics

Hα and the Ca II H and K lines as activity proxies for late-type stars⋆

C. Cincunegui[1,2,⋆⋆], R. F. Díaz[1,2,⋆⋆], and P. J. D. Mauas[1,3,⋆⋆]

[1] Instituto de Astronomía y Física del Espacio, CONICET-UBA, C.C. 67 Suc. 28 (1428) Buenos Aires, Argentina
e-mail: carolina@iafe.uba.ar
[2] Fellow of the CONICET
[3] Member of the Carrera del Investigador Científico, CONICET

Received 3 October 2006 / Accepted 14 March 2007

ABSTRACT

Context. The main chromospheric activity indicator is the S index, which is the ratio of the flux in the core of the Ca II H and K lines to the continuum nearby, and is well studied for stars from F to K. Another chromospheric proxy is the Hα line, which is believed to be tightly correlated with the Ca II index.
Aims. In this work we characterize both chromospheric activity indicators, the one associated with the H and K Ca II lines and the other with Hα, for the whole range of late type stars, from F to M.
Methods. We present periodic medium-resolution echelle observations covering the complete visual range, taken at the CASLEO Argentinean Observatory over 7 years. We use a total of 917 flux-calibrated spectra for 109 stars that range from F6 to M5. We statistically study these two indicators for stars of different activity levels and spectral types.
Results. We directly derive the conversion factor that translates the known S index to flux in the Ca II cores, and extend its calibration to a wider spectral range. We investigate the relation between the activity measurements in the calcium and hydrogen lines, and found that the usual correlation observed is the product of the dependence of each flux on stellar colour, and not the product of similar activity phenomena.

Key words. stars: late-type – stars: activity – stars: chromospheres

1. Introduction

In the Sun, the magnetic fields that are generated by turbulence in the outer convection zone and penetrate the solar atmosphere cause a very broad range of phenomena, such as sunspots, plages, active regions, flares, etc. The term stellar activity refers to similar features that occur in late-type stars, i.e., in stars that also have an outer convection zone. It is generally accepted that magnetic activity in late-type stars is the product of an $\alpha\Omega$ dynamo, which results from the action of differential rotation at the tachocline (the interface between the convective envelope and the radiative core).

Therefore, the nature of stellar activity is closely related to the existence and depth of an outer convection zone. Since this depth depends on spectral type – from F stars which have shallow convection zones to middle M stars which are totally convective –; it is of special interest to characterize the stellar activity in stars of different spectral types.

To date, the most common indicator of chromospheric activity is the well-known S index, esentially the ratio of the flux in the core of the Ca II H and K lines to the continuum nearby (Vaughan et al. 1978). This index has been defined at the Mount Wilson Observatory, were an extensive database of stellar activity has been built over the last four decades. However, these observations are mainly concentrated on stars ranging from F to K (see, for example, Baliunas et al. 1995), due to the long exposure times needed to observe the Ca II lines in the red and faint M stars. For this reason, the S index is poorly characterized for these stars. In spite of that, many attempts have been made to study activity using the Ca II lines (see, for example Pasquini et al. 1989; Duncan et al. 1991; Henry et al. 1996; Wright et al. 2004).

Nevertheless, as we pointed out, the H and K lines are not the most adequate activity indicator for K and M stars, due both to their red color and to their intrinsically faint luminosity. Another well studied activity indicator is the Hα line (see, for example Pasquini & Pallavicini 1991; Montes et al. 1995). It has been claimed that a strong correlation exists between Hα and the Ca II lines (Montes et al. 1995; Strassmeier et al. 1990; Robinson et al. 1990; Giampapa et al. 1989).

In this work we characterize both chromospheric indicators for a sample of more than 100 Southern stars. We use more than 900 flux-calibrated spectra which include the full spectral range between both proxies.

The paper is organized as follows. In Sect. 2 we explain how we choose the stellar sample and present the observations, and briefly describe the method employed to calibrate them. In Sect. 3 we analyze the Ca II lines and its continuum nearby; the Hα line and its continuum are studied in Sect. 4. Since in our spectra both fluxes are measured simultaneously, we are able to study in detail the correlation between the Ca II lines and Hα.

⋆ Tables 1 and 2 and full Figs. 1 and 6 are only available in electronic form at http://www.aanda.org

⋆⋆ Visiting Astronomers, Complejo Astronómico El Leoncito operated under agreement between the Consejo Nacional de Investigaciones Científicas y Técnicas de la República Argentina and the National Universities of La Plata, Córdoba and San Juan.

We perform this analysis in Sect. 4. In Sect. 5 we summarize our results.

2. The observations

2.1. The sample of stars

We study a sample of 109 Southern stars chosen to cover the whole range of depths of the convective zone ($0.45 \leq B-V \leq 1.81$), from the onset of the outer convective layer to fully convective stars. They were also selected to include different levels of chromospheric activity, from stars known to have non varying records to flare stars.

In Table 2 we list the stars included in the sample. For each star we give the HD and GJ/GL numbers and the star name. In the fourth column we indicate which stars are expected to be particularly active, either because they are dMe stars or because they belong to the RS CVn or the BY Dra types. We also specify which stars are chosen as non-variable by Henry et al. (1996), based on the long-term observations of the Mount Wilson database of the Ca II lines. Also indicated are the stars for which planetary systems have been reported.

In the fifth to seventh columns we list the star's spectral type, its V magnitude and $B-V$ colours, taken from Perryman et al. (1997), except for the ones indicated. From the same catalogue we give the parallaxes (in mas). The gravity and metallicity are taken from Cayrel de Strobel et al. (1997, 2001). The eleventh column lists the rotational periods, either measured or estimated from $v \sin i$, as stated. In column number twelve we include the number of observations of each star used in this work.

In the last five columns we give the mean activity indexes $\langle S \rangle$ (in Mount Wilson units), $\langle F_{\rm HK} \rangle$ and $\langle F_{\rm H\alpha} \rangle$, as defined in Sects. 3.2 and 4.2, and the parameters of the linear regresions of Sect. 4.3.

2.2. The observations and their processing

Our observations were made with the 2.15 m telescope of the Complejo Astronómico El Leoncito (CASLEO), which is located at 2552 m above sea level, in the Argentinian Andes. The medium-resolution echelle spectra were obtained with a REOSC spectrograph designed to work between 3500 and 7500 Å and a 1024 × 1024 pixel TEK CCD as detector. The maximum wavelength range of our observations is from 3860 to 6690 Å ($R = \lambda/\delta\lambda \approx 26\,400$).

We calibrated in flux all the spectra following the procedure described in Cincunegui & Mauas (2004). The method makes use of long-slit spectra of the same target stars. We calibrated these low-resolution spectra with spectrophotometric standard stars by the usual procedure. Then, for each echelle spectrum, we flux-calibrated it using the long-slit spectrum of the same star as if it were a standard star. In Cincunegui & Mauas (2004) there are various examples of these spectra, together with a discussion about the errors involved in the calibration procedure.

We began our observing program in 1999, and at present we carry on four to five observing runs per year. In this work we use a total of 917 spectra for 109 stars.

3. Ca II index

The index most extensively used for chromospheric activity studies is the well known Mount Wilson S index. Nevertheless, it is not well characterized for the less masive stars. As we explained, because of the long exposure times needed to observe these stars, they are usually not included in the stellar activity databases. In this section we study the behaviour of the S index in the whole range of stars with a radiative core and a convective outer layer, i.e., from mid F to mid M.

In Fig. 1 we show the windows chosen to integrate the fluxes in the Ca II region, as explained in the next subsections, for several stars of different spectral types and different activity levels.

3.1. Calibration of the Ca II continuum

Several authors have constructed empirical stellar fluxes scales, relating observed stellar properties, such as colour indexes, to the surface flux in specific bandpasses. For example, Linsky et al. (1979) found a relation between the Johnson $V-R$ and the surface flux in the 3925–3975 Å bandpass. Pasquini et al. (1988) developed an empirical calibration for the flux at the Ca II H and K lines, and Pasquini & Pallavicini (1991) did something similar for the flux close to the Hα line. Hall et al. (1995) derived the flux in the Ca II infrared triplet, H and K lines and Hα as a function of $b-y$, and Hall (1996) have constructed empirical fluxes for the continuum near Ca II H and K and Hα as a function of different colour indexes. These results apply to F-K dwarfs.

To derive a calibration for the Ca II continuum directly from our flux-calibrated observations, we integrated the continuum flux (as measured from Earth) in two passbands near the center of the Ca II lines, defined in a similar way as the continuum passbands of the Mount Wilson Observatory: the blue window is centered at 3891 Å and the red one at 4011 Å, and both of them are 20 Å wide. We average these quantities to obtain a mean flux at the continuum, $f_{\rm BR}$, and we converted it to an absolute stellar flux, $F_{\rm BR}$ (Cox 2000):

$$F_{\rm BR} = \frac{4\pi\sigma {T_{\rm eff}}^4}{L_\odot} (10\,{\rm pc})^2\, 10^{(V+BC-M_{\rm bol}^\odot)} f_{\rm BR}\,, \qquad (1)$$

where we used the values given in Johnson (1966) to interpolate the effective temperature $T_{\rm eff}$ and the bolometric correction BC as functions of $B-V$. 62 of the stars of our sample have measurements of $T_{\rm eff}$ from Cayrel de Strobel et al. (1997, 2001) and Ségransan et al. (2003). For these stars, in Fig. 2 we compare the measured $T_{\rm eff}$ with the one estimated from the interpolation of Johnson's data. The fit shown in the lower panel is given by

$$\text{estimated}\, T_{\rm eff} = -145.5 + 1.01 \text{measured}\, T_{\rm eff}\,, \qquad (2)$$

with a correlation coefficient $\rho = 0.98$. The scatter in the graph is smaller than 5%, and is independent of spectral type.

In Fig. 3 we plot the absolute mean continuum flux given by Eq. (1) as a function of colour. For the rest of the work, the F stars are indicated with triangles pointing downwards, the G stars with diamonds, the K stars with triangles pointing upwards and the M stars with squares.

As can be seen, two K stars clearly depart from the general trend: the bluer is HD156425, and the redder HD94683. This star was included in our sample because it was classified as a K5V star in the SIMBAD database. Nevertheless, according to Perryman et al. (1997) its luminosity class is III. We can therefore confirm that it is evolved. With regard to HD156425, its parallax is unknown, so we cannot assure its luminosity class. Both stars were discarded in the subsequent analysis.

We performed a least-squares fit with a quadratic function, considering errors of 10% in the flux, and obtained:

$$\log F_{\rm BR} = 7.739 - 0.842\,(B-V) - 0.760\,(B-V)^2 \qquad (3)$$

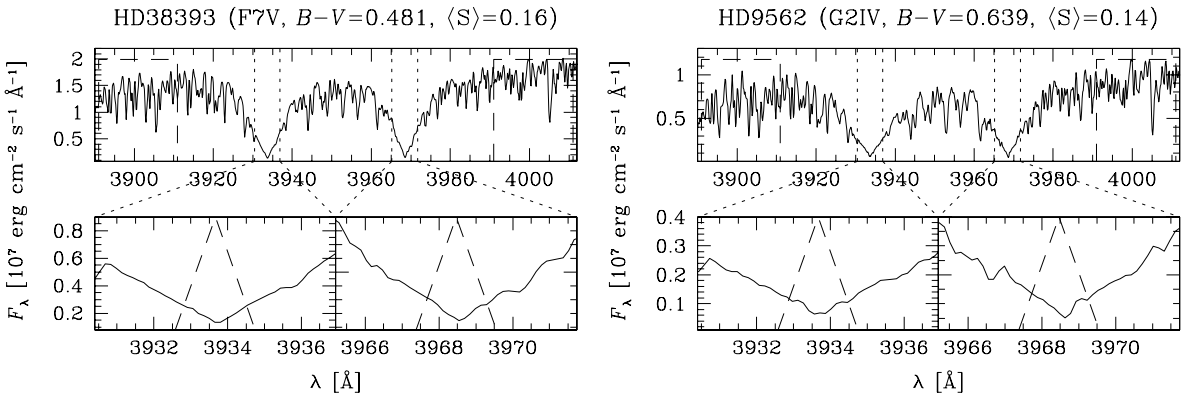

Fig. 1. Windows used to compute our S' index, for six stars of different spectral types and activity levels. For each star, we show in the top panel the whole spectral range used, with the continuum windows indicated with dashed lines. Below each of these spectra, we show in detail the H and K lines, and the triangular shape used to integrate the fluxes.

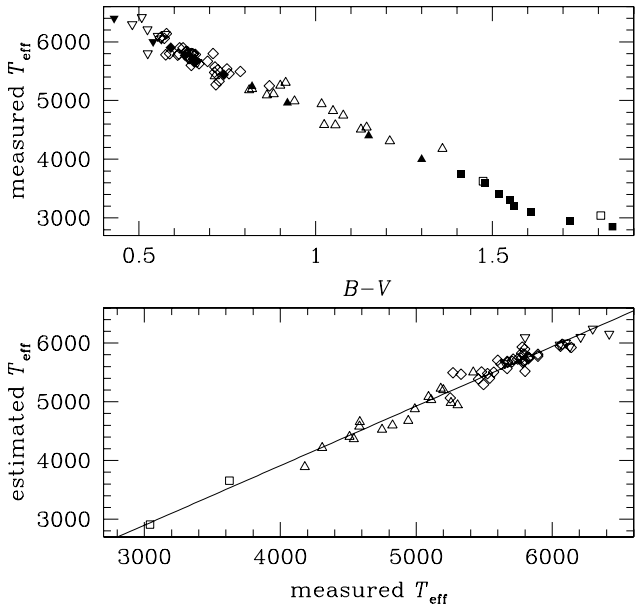

Fig. 2. In the *upper panel*, we show in open symbols the measured $T_{\rm eff}$ for 62 stars of our sample, taken from Cayrel de Strobel et al. (1997, 2001) and Ségransan et al. (2003). The filled symbols correspond to the data used to interpolate, from Johnson (1966). The *lower panel* shows the $T_{\rm eff}$ calculated from the interpolation as a function of the measured $T_{\rm eff}$, for these 62 stars. The fit is given by Eq. (2). As in the rest of the figures, the symbols ▽, ◊, △ and □ represent F, G, K and M stars respectively.

with an error given by

$$\sigma_{[\log F_{\rm BR}]} = 10^{-2}\Big[2.04 - 8.38\,(B-V) + 12.59\,(B-V)^2 - 8.06\,(B-V)^3 + 1.88\,(B-V)^4\Big]^{0.5}\,. \quad (4)$$

The function is shown as a full line in Fig. 3, and the dotted lines represent the $\pm 3\sigma$ bands. This fit has a significance of 99.99%, considering the 742 spectra with B–$V \leq 1.2$. This significance is greatly reduced, however, if all the 886 spectra, are considered, due to the small number of spectra with $B-V > 1.2$ and the increased spread for these points.

It is possible to introduce a bias in this fit, due to the inhomogeneous distribution in colour of our stellar sample, and to the different number of observations for each star. To investigate

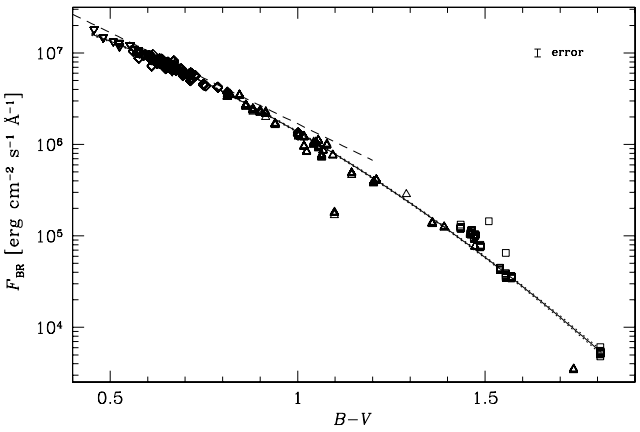

Fig. 3. $F_{\rm BR}$ as a function of colour. The solid line is a least-squares fit to the stars excluding HD 156425 and HD 94683, given by Eq. (3). The dashed line is the relation found by Hall (1996).

this, we averaged the measurementes in bins of 0.1 in colour – excluding HD 156425 and HD 94683 –, to account for the bias induced by the larger number of stars with $B-V \leq 1.2$. We computed the errors as the standard deviation within each bin, since the bins are narrow enough to contain only stars with very similar photospheres. Finally, we fitted the results with a quadratic function. The differences to Eq. (3) were always smaller than 15%.

Hall (1996) also studied the behaviour of the continuum flux at 3950 Å, compiling spectrophotometric data of several authors. He found:

$$\log(F_{3950})_{\rm Hall} = [-1.995\ (B-V) + 8.221] \pm 0.045\,, \quad (5)$$

for a sample smaller than 95 dwarf stars with $-0.1 \leq B$–$V \leq 1.2$. This fit is shown as a dashed line in Fig. 3. The difference between expressions is probably due to two different facts that have the opposite effect.On one hand, the chosen continuum is not the same. At 3950 Å what is measured is a "pseudo-continuum": the Ca II lines are so wide that at that wavelength still exists some absorption. Our flux, measured far away from the cores, is more intense, and is a more realistic estimation of the true continuum, since the contribution of the line absorption is smaller. On the other hand, Hall (1996) corrected the fluxes for the blanketing coefficients and we did not, which should result in our fluxes being smaller.

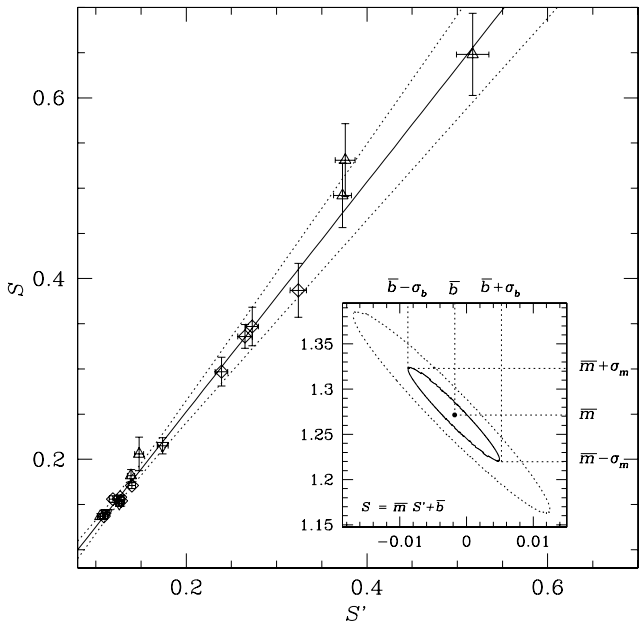

Fig. 4. S index, as measured at Mount Wilson, as a function of our mean S' index, for the 18 stars chosen as reference stars. The full line is a least-squares fit, and the dotted lines are the $\pm 3\sigma$ curves. In the insert we indicate the 39.3% confident level (full line) and the 90% confidence level (dotted line) for the two parameters fitted.

We also performed a linear fit, as was done by Hall (1996). However, for the stars with B–$V \leq 1.2$ the significance of the linear fit is reduced to 95%. For this reason, we prefer the quadratic form given in Eq. (2).

3.2. Calibration of the S index

As far as we know, the only work that compiles measurements of the index S for Southern stars is the one from Henry et al. (1996). They observed more than 800 stars with a Cassegrain Spectrograph. Although our sample of stars is smaller, we have collected several observations for each star, which allows us to study the behaviour in time of a particular star (see, for example Cincunegui et al. 2007). Our sample of stars spans a wider range in spectral type, since Henry et al. only studied stars with $0.5 \leq B-V \leq 1.0$.

We have defined an S' index in a similar way as the one used in Mount Wilson: we integrated the flux in two windows centered on the cores of the Ca II H and K lines, weighted with triangular profiles of 1.09 Å *FWHM* to mimic the response of the Mount Wilson instrument, and computed S' as the ratio between this average line flux and the one at the continuum defined in the previous section.

In order to corroborate the accuracy of this definition, we have included in our sample 18 stars from the Mount Wilson database defined as non-variable by Henry et al. (1996), and we have observed each of these stars between 8 and 14 times. In Fig. 4 we plot the Mount Wilson S index as a function of our mean S' for these stars, calculated by weigthing each individual measurement with an error of 10%. The data used for this figure are presented in Table 1. We performed a least-squares fit, obtaining:

$$S = (1.271 \pm 0.052)\, S' - (0.002 \pm 0.007)\,, \tag{6}$$

with a correlation coefficient of −0.96. The significance of the fit is greater than 87%. As can be seen in Table 1, the color range involved in this calibration goes from $B-V = 0.48$ to $B-V = 0.94$, only a portion of the whole color range of our sample, $0.45 \leq B-V \leq 1.81$. Therefore, this technique allows us to reproduce the Mount Wilson measurements with our instrument, with high confidence for stars with $B-V < 1$, and with some uncertainty for the whole sample. Since there are no available systematic measurements of M stars, we cannot estimate the errors introduced by this procedure.

3.3. Conversion factor between S and the flux

The Mount Wilson S index can be converted to the average surface flux in the Ca II lines through the relation:

$$F_{\rm HK} = F_{\rm bol} 1.34 \times 10^{-4}\, S\, C_{\rm cf}\,, \tag{7}$$

where $C_{\rm cf}\,(B-V)$ is a conversion factor that depends on colour. Two different expressions are widely used for this factor, the first one given by Middelkoop (1982) and corrected by Noyes et al. (1984) and the other one given by Rutten (1984). The deductions used in both works to derive $C_{\rm cf}$ involve complex calibration procedures.

The conversion factor computed by Middelkoop and Noyes et al. is valid for $0.45 \leq B-V \leq 1.5$, and is given by:

$$\log\, C_{\rm cf}^{\rm MN} = 1.13\, y^3 - 3.91\, y^2 + 2.84\, y - 0.47 + \Delta \tag{8}$$

where $y \equiv (B-V)$ and the last term is, as a function of $x \equiv 0.63 - (B-V)$:

$$\Delta\,(x) = \begin{cases} 0 & \text{if } x < 0 \\ 0.135\, x - 0.814\, x^2 + 6.03\, x^3 & \text{if } x > 0\,. \end{cases} \tag{9}$$

On the other hand, the conversion factor computed by Rutten is:

$$\log\, C_{\rm cf}^{\rm R} = 0.25\, y^3 - 1.33\, y^2 + 0.43\, y + 0.24 \tag{10}$$

and it is valid for main-sequence stars with $0.3 \leq B-V \leq 1.6$. These conversion factors have also been used in recent works (see, for example, Wright et al. 2004).

Since we have simultaneous measurementes of the S index and the core fluxes, we can calculate directly the correction factor as a function of the index and the flux, fitting the expression:

$$\log C_{\rm cf} = \log F_{\rm HK} - \log \sigma T_{\rm eff}^4 - \log S - \log 1.34 + 4\,, \tag{11}$$

were we have obtained S as a function of the measured S' using Eq. (6).

In Fig. 5 we plot the correction factor computed from Eq. (11) as a function of colour. The full line corresponds to a least-squares fit to the data, with a significance higher than 99% for the 880 spectra included. This fit is given by:

$$\log C_{\rm cf} = -0.33y^3 + 0.55y^2 - 1.41y + 0.8\,, \tag{12}$$

where $y \equiv B-V$, and the errors of the fit are:

$$\sigma_{[\log C_{\rm cf}]} = \left[0.24 - 1.48y + 3.65y^2 - 4.7y^3 + 3.34y^4 - 1.24y^5 + 0.19y^6\right]^{1/2} 10^{-1}. \tag{13}$$

This fit is valid for the whole range $0.45 \leq B-V \leq 1.81$. Also shown in the same figure are the conversion factors of Middelkoop (1982) and Noyes et al. (1984, dashed line) and Rutten (1984, dotted line). The three conversion factors are very similar for stars with $0.6 \leq B-V \leq 1.0$, which are the most

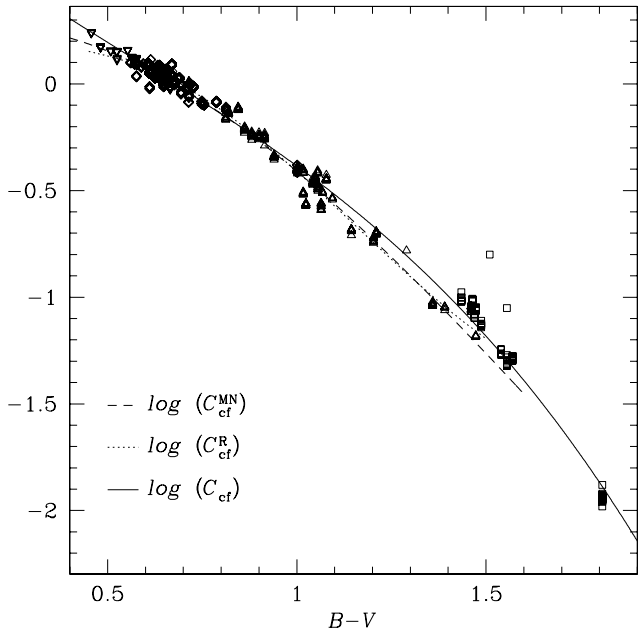

Fig. 5. Conversion factor between Mount Wilson S index and $F_{\rm HK}$. The dashed line corresponds to Noyes et al. (1984), the dotted line to Rutten (1984), and the full line to our derived factor, Eq. (12). The stars HD 156425 and HD 94683 have been discarded.

crowded of our sample. Our factor lies slightly apart from the others for $1.0 \leq B-V \leq 1.5$, while it extends the calibration up to $B-V = 1.8$.

The conversion factor of Eq. (12) was derived using spectra that were calibrated in flux, the same as were used to measure the S index. On the other hand, the ones given by Middelkoop (1982) and Noyes et al. (1984), and Rutten (1984), were computed using interpolated fluxes at the appropiate wavelengths from other instruments.

3.4. The photospheric contribution

The S index depends both on the chromospheric and photospheric radiation, while the activity is related only to the chromospheric part. This dependence of S is due, in the first place, to the flux in the continuum windows, which is a strong function of the spectral type. Furthermore, the passbands centered on the cores of the lines include some photospheric contribution from the flux, in particular outside the H_1 and K_1 minima. For these reasons it is usually considered that a better indicator of chromospheric activity is $R'_{\rm HK}$, defined as:

$$R'_{\rm HK} = \frac{F_{\rm HK} - F_{\rm phot}}{F_{\rm bol}}\,, \tag{14}$$

where $F_{\rm HK}$ is the average surface flux in the center of the H and K lines, $F_{\rm phot}$ is the photospheric contribution integrated in the lines and $F_{\rm bol} = \sigma T_{\rm eff}^4$.

The triangular profiles used to integrate the line fluxes $F_{\rm HK}$ include some flux outside the H_1 an K_1 minima, which is formed in the stellar atmosphere below the temperature minimum. This flux of photospheric origin, $F_{\rm phot}$, introduces a dependence on stellar colour which has to be substracted in order to obtain the net chromospheric line flux $F'_{\rm HK}$ defined as:

$$F'_{\rm HK} = F_{\rm HK} - F_{\rm phot}\,. \tag{15}$$

Unfortunately, our instrumental resolution is not good enough to measure the photospheric flux in this way.

We have adopted instead the functional form proposed by Noyes et al. (1984):

$$\log\left(\frac{F_{\rm phot}}{F_{\rm bol}}\right) = -4.02 - 1.40\,(B-V)\,, \tag{16}$$

in the range $0.44 < B-V < 0.82$. This expression has been derived for the Mount Wilson survey. As the authors explain in the cited work, they have also used the same form for$B-V > 0.82$. In fact, it becomes negligible for $B-V \gtrsim 1.0$, so we extrapolated it to our full range of colours. We will use this expression to obtain the chromospheric flux used for the analysis of Sect. 4.3.

4. Hα index

Although the Ca II resonance lines have been the most widely used chromospheric indicators, they present two problems when they are used to study cool stars. First, the coolest stars – mid K to mid M – are progressively redder than the hottest ones, and therefore the spectral range where these lines are located becomes less intense relative to other ranges of the visual spectrum as the temperature decreases. Moreover, these coolest stars are instrinsically faint, and therefore this problem is increased. As a consequence, the Ca II lines are not the best suited to observationally study the coolest stars of our sample, because the signal-to-noise ratio for these lines is very small, even with long exposure times.

Although in most solar-type dwarfs the formation of the Hα line is dominated by photoionization, as we move to later stars the decrease in the photospheric radiation temperatures gives way to a significant collisional contribution to the source function and eventually Hα goes into emission for the dKe and dMe stars (Thatcher & Robinson 1993; Mauas & Falchi 1994; Mauas et al. 1997). Therefore, Hα is also usually used as a chromospheric indicator (Labonte 1986; Pasquini & Pallavicini 1991; Thatcher & Robinson 1993; Montes et al. 1995; Hall et al. 1995). Furthermore, the spectral location of this line is much more adequate for late stars and the integration times needed to obtain a proper signal-to-noise ratio are much lower than for the Ca II lines.

In Fig. 6 we show the windows of interest for Hα for the same stars as in Fig. 1. In the next subsections we explain how we used these observations.

4.1. Calibration of the Hα continuum

In a similar way to the calcium index, we choose two windows to integrate the fluxes, one centered in the line and the other in the continuum nearby. We calibrated the continuum for this line as we did in Sect. 3.1, on one hand, to corroborate the quality of the flux-calibration in the Hα region and, on the other, because an expression of this kind can be used to calibrate normalized spectra in this spectral region.

We measured the continuum flux averaged in a window 20 Å wide centered at 6605 Å, and we translated it to surface flux, using an equation similar to Eq. (1). It is plotted as a function of colour in Fig. 7. $B-V$ is not the best $T_{\rm eff}$ proxy for the coolest stars, as can be seen from the wide scatter for the later stars of Fig. 7, but it is the only color index available for our whole sample of stars. Since this calibration can induce errors in the Hα flux, we restrict our analysis to stars with $B-V \leq 1.4$, and we indicate the stars excluded from the analysis with a note in

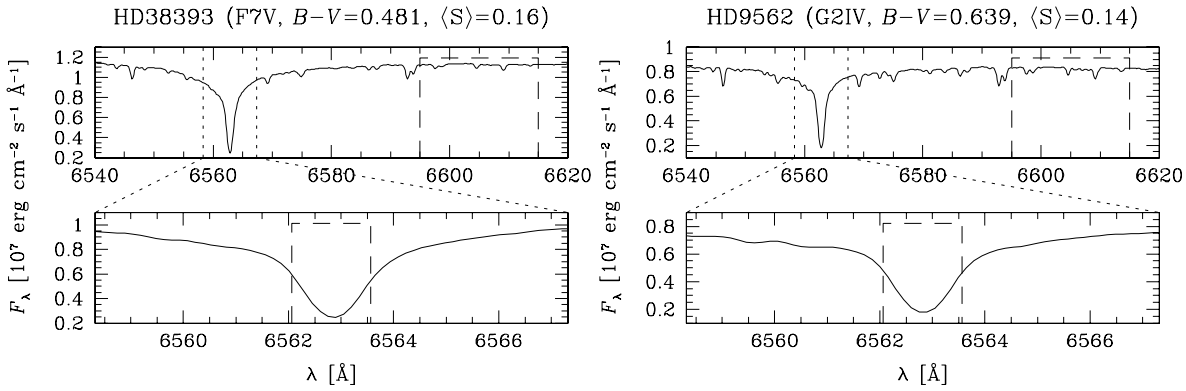

Fig. 6. Windows used to measure the fluxes in Hα, for six stars of different spectral types and activity levels, the same as in Fig. 1. For each star, we show in the top panel the whole range used, with the continuum window indicated with dashed lines. Below each of these spectra, we show in detail the Hα line, superimposed on the filter used to integrate the fluxes.

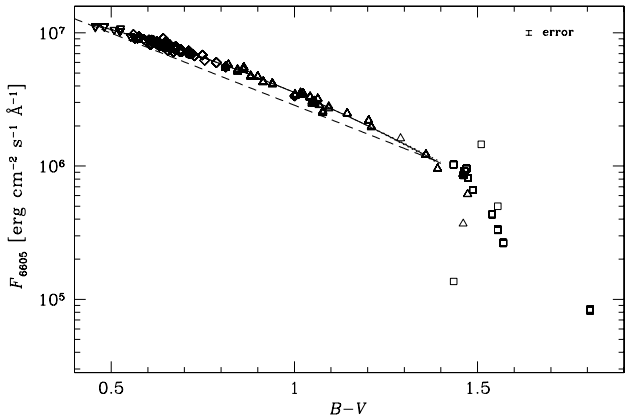

Fig. 7. F_{6605} as a function of colour. The dashed line is the relation found by Hall (1996).

Table 2. For the 783 points corresponding to these stars we found:

$$\log F_{6605} = 7.281 - 0.298\,(B-V) - 0.431\,(B-V)^2\ , \qquad (17)$$

with errors:

$$\sigma_{[\log F_{6605}]} = 10^{-2}\left[1.06 - 5.08\,(B-V) + 8.97\,(B-V)^2 - 6.96\,(B-V)^3 + 2.00\,(B-V)^2\right]^{0.5} \qquad (18)$$

and a significance of 84%, assuming individual errors of 4%. This fit is drawn with a full line in the figure. Hall (1996) compiled data from different sources of spectrophotometry, and, using a method that interpolates the continuum flux to the wavelength of the line center, found a similar behaviour:

$$\log\,(F_{6563})_{\rm Hall} = [-1.081(B-V) + 7.538] \pm 0.033\ {\rm dex}\,, \qquad (19)$$

which is marked with a dashed line in the same figure.

4.2. Hα flux and its photospheric contribution

We computed the flux in the Hα line, $F_{\rm H\alpha}$, as the average surface flux in a 1.5 Å square passband centered on the line. Pasquini & Pallavicini (1991) studied the flux on the stellar surface in a 1.7 Å window centered at Hα, for a sample of G and K dwarf stars, 24 of which were also included in our sample. For these stars, we calculated $\langle F_{\rm H\alpha}\rangle$, the average flux in the line, shown in Fig. 8. By means of a least-squares fit, we find that the Pasquini & Pallavicini fluxes $F^{\rm PP}_{\rm H\alpha}$ are related to ours $\langle F_{\rm H\alpha}\rangle$ by:

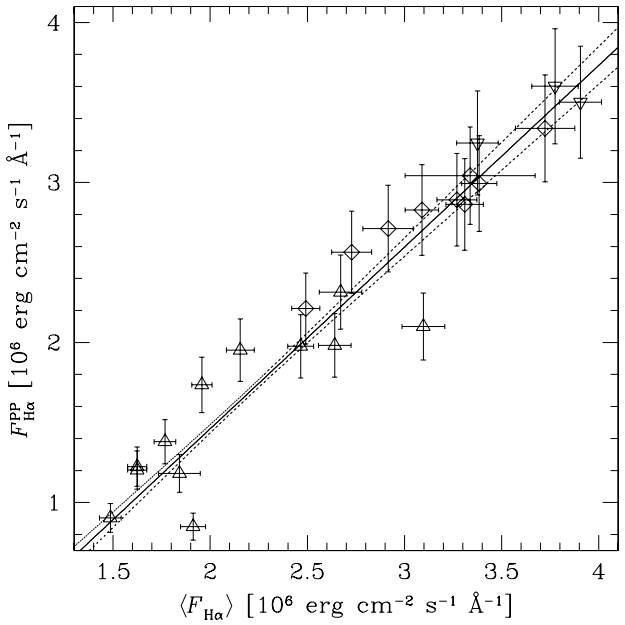

Fig. 8. Average surface flux in the center of Hα, for the 24 stars in common between our sample ($\langle F_{\rm H\alpha}\rangle$) and the one of Pasquini & Pallavicini (1991, $F^{\rm PP}_{\rm H\alpha}$). The full line corresponds to a least-squares fit of the data, and the dashed line to the $\pm 3\sigma$ band.

$$F^{\rm PP}_{\rm H\alpha} = (1.136 \pm 0.063)\,\langle F_{\rm H\alpha}\rangle - (0.811 \mp 0.139)\,, \qquad (20)$$

where Pasquini & Pallavicini values have 10% errors, and we have considered the *individual* errors of our measurements to be 10% as well. However, since we have between 5 and 14 observations for most stars, the errors in Fig. 8 are much smaller.

As it can be seen in Fig. 8, the correlation between both sets of measurements is excelent, particularly considering that our fluxes and the Pasquini & Pallavicini ones were taken at different moments, i.e. with different levels of activity.

To estimate the photospheric contribution to this line is much more complicated than for the calcium ones. On one hand, for the Ca lines one can determine where in the wings the flux is of photospheric origin. On the other, the photospheric contribution to the Ca II line fluxes is less important than the chromospheric one, while the center of the Hα line is clearly not opaque

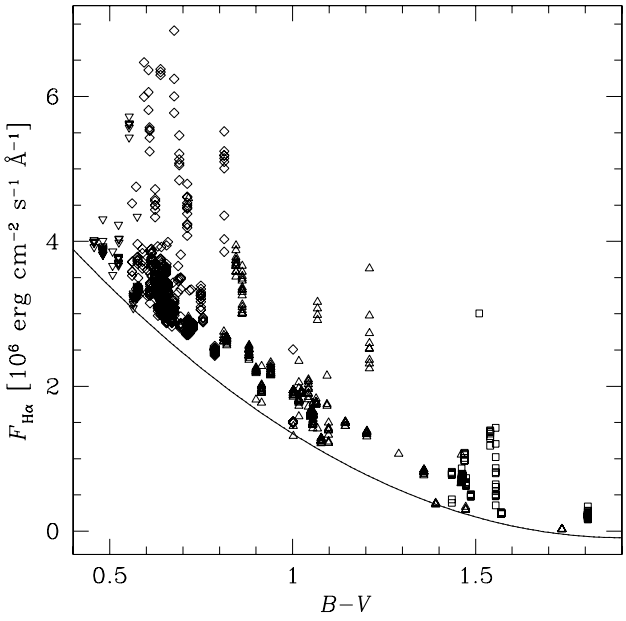

Fig. 9. Average surface flux in the center of Hα as a function of colour, for the whole sample of stars. The full line represents the minimum flux given by Eq. (21).

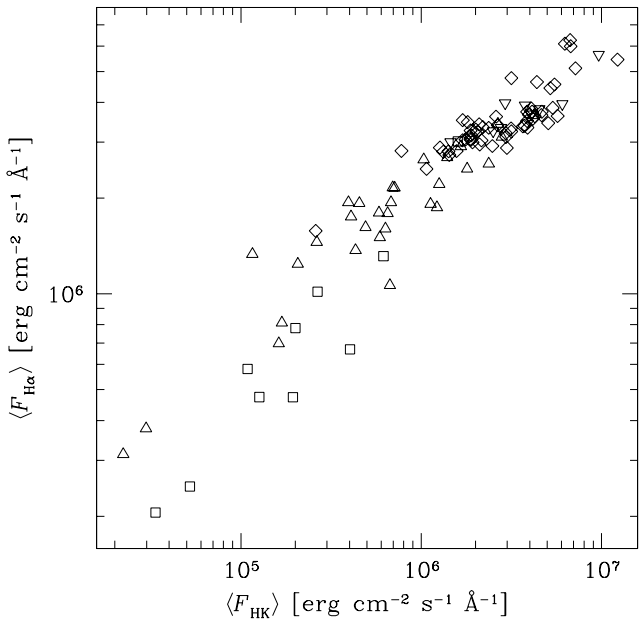

Fig. 10. Average Hα surface fluxes as a function of the average Ca II surface fluxes.

even for the least active stars, and therefore in this case the chromospheric contribution is the result of a subtraction of two comparable quantities.

The usual way of overcoming this problem, when the number of observations is large enough, is to assume that the photospheric flux depends only on stellar colour and corresponds to the minimum flux observed. In Fig. 9 we show $F_{H\alpha}$ as a function of $B-V$. The full line is the curve that represents the minimum flux of the line, which we fit with a quadratic polynomial of the form:

$$F_{H\alpha}^{min} = 10^4 \left[629 - 670\,(B-V) + 176\,(B-V)^2\right]. \quad (21)$$

4.3. Relation between the Ca II and Hα fluxes

It is usually accepted that there is a tight relation between the chromospheric fluxes emitted in Hα and in the H and K Ca II lines. However, most works where this relation has been observed (see, for example, Giampapa et al. 1989; Robinson et al. 1990; Strassmeier et al. 1990; Montes et al. 1995) found it by using averaged fluxes for both the calcium and the hydrogen lines, which were not obtained simultaneously, and were even collected from different sources. Thatcher & Robinson (1993), on the other hand, did use simultaneous observations, which represent a particular moment of each star and not an average behaviour, but they observed each star only once.

In Fig. 10 we have reproduced this kind of study averaging for each star our measurements of the Ca II and the Hα fluxes, obtained by direct integration of the spectra, and weighting them with their individual errors. For the 108 points shown there is a clear correlation between both fluxes, especially for the stars whith the strongest chromospheric emission.

However, the situation is different when the individual stars are studied separately. In Fig. 11 we plot the individual simultaneous measurementes of each flux for several stars of different spectral types and different levels of activity, divided into color bins as stated. The error bars represent the 10% of uncertainty we assign to our flux calibration, as explained in Cincunegui & Mauas (2004). We also show the linear fits for each star. It can be seen that the behavior is different in each case: in some stars both fluxes are well correlated, as in HD 118100 and HD 36395, although the slopes of the fits are not the same. In other stars such as HD 30495 $F_{H\alpha}$ seems to be almost independent of the level of activity measured in the Ca II lines, and there are even stars like HD 151770 where the fluxes are anti-correlated.

We found no evidence of dependence of this behaviour on spectral type or level of activity. Even when we restrict the analysis to dMe stars, where the mechanisms of formation of the lines are supposed to be similar, the behaviour differs for different stars: for example, for GL551 (Prox Cen) we found a good correlation for both fluxes (see Cincunegui et al. 2007, where the study was made much more carefully, taking into account variations produced by flares) while for GL699 (Barnard's star) Hα seems to be independent of the activity measured by Ca II. In Table 2 we included in the last two columns the slopes and correlation coefficients of these fits. It can be seen that there is no clear indication of how Hα varies with Ca II.

This fact seems to indicate that the trend present in Fig. 10 is not the product of a direct relationship between the activity measured in Hα and in the Ca II lines, but is due to a correlation of each separate flux with the stellar colour or the spectral type.

In Fig. 12 we plot the fluxes directly related to the chromospheric activity, $\langle F_{HK} - F_{HK}^{phot} \rangle$ and $\langle F_{H\alpha} - F_{H\alpha}^{min} \rangle$, where we used Eqs. (16) and (21) to compute F_{HK}^{phot} and $F_{H\alpha}^{min}$ respectively. We see that the correlation becomes much more unclear and the spread much larger. Soderblom et al. (1993) have already argued that, given the different conditions of formation of Hα and the H and K lines, it is possible to find significant differences between their behaviour when observing two different stars, since the underlying physics for each line could differ much between them.

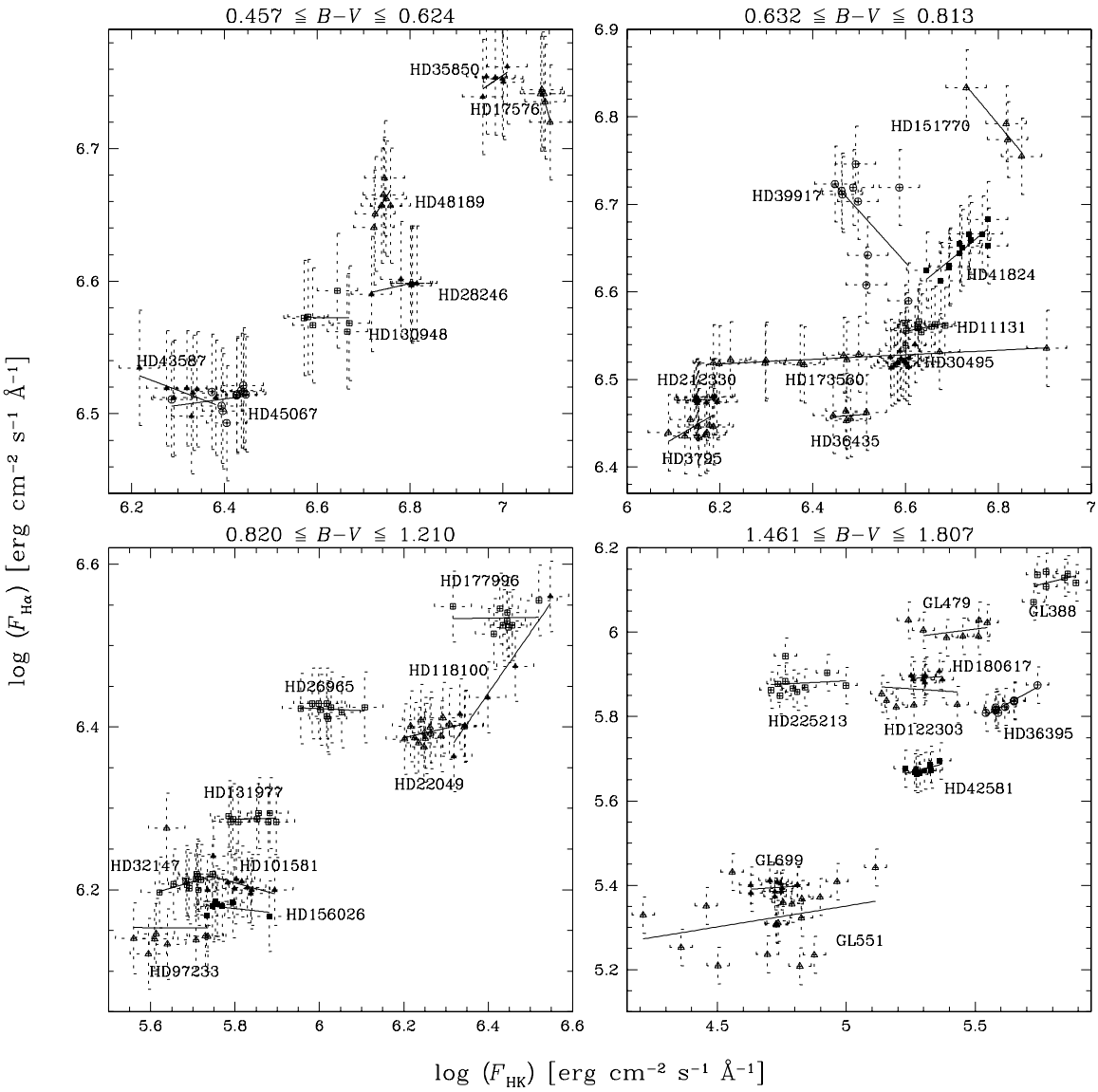

Fig. 11. Hα surface fluxes as a function of the Ca II surface fluxes, for stars of different spectral types, divided into different color bins, as indicated.

5. Summary

This work concentrates on the statistical study of two activity indicators for stars of different activity levels and spectral types. We use mid-resolution spectra calibrated in flux for 109 Southern stars from F6 to M5. We have a total of 917 simultaneous observations of these stars, which range from Ca II H and K to the Hα region.

The first indicator we have characterized is the one related to the H and K Ca II lines. We studied the dependence of the continuum flux near these lines with colour, and we found an excellent agreement with similar studies by other authors, corroborating the quality of our observations and reduction techniques. Using 18 stars selected because of their small variability, our S' index correlates very well with the index from the Mount Wilson Observatory, which allows us to intercalibrate both sets of measurements.

Usually, the S index is measured with the Mount Wilson instrument or from normalized spectra, and a conversion factor is computed –through indirect calibrations– to translate the index to the flux in the line. To our knowledge, this is the first work where the S index is measured from flux-calibrated spectra, a fact that allows us to have simultaneous observations of the index and of the flux in the lines. Taking adventage of this fact, we derived the conversion factor between S and the line flux directly, and extended it to a wider colour range.

We also studied the behaviour of the flux in the Hα region. We first explored the relation of the continuum flux with colour reproducing very well previous results in the literature. In this case we also found an excellent match between our flux in the line and the fluxes published by other authors, for 24 stars of the sample.

Usually the Hα and Ca II fluxes are used interchangeably as activity indicators. Since we have a large number of simultaneous observations of both fluxes we could explore their correlation in detail. We found a strong correlation between the mean fluxes of each line for each star. However, when we investigate this relation for individual observations of particular stars, the general trend is lost and each star shows a particular behaviour, ranging from tight correlations with different slopes to anti-correlations, including cases where no correlations are found. We found no evidence of dependence of this behaviour on spectral type or level of activity.

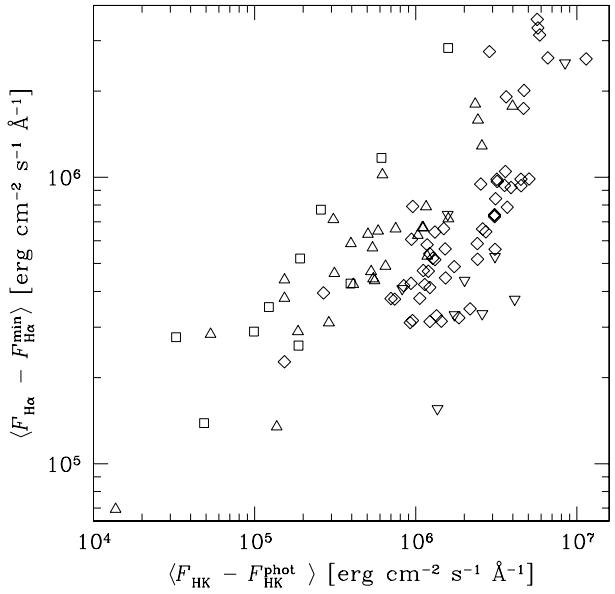

Fig. 12. Average surface fluxes of chromospheric origin, for Hα and the H and K lines. The close relation of Fig. 10 has a much larger spread.

We conclude that the close relationship for the mean values is the product of the dependence of the mean fluxes on stellar colours. Therefore, we found that in general the activity measured in Hα is not equivalent to the one measured in the Ca II lines for the whole sample of stars.

Acknowledgements. The CCD and data acquisition system at CASLEO has been partly financed byR. M. Rich through U.S. NSF grant AST-90-15827. This work made extensive use of the SIMBAD database, operated at CDS, Strasbourg, France. We thank the anonymous referee for his/her useful comments.

References

Baliunas, S. L., Donahue, R. A., Soon, W. H., et al. 1995, ApJ, 438, 269
Baliunas, S., Sokoloff, D., & Soon, W. 1996, ApJ, 457, L99
Cayrel de Strobel, G., Soubiran, C., Friel, E. D., Ralite, N., & Francois, P. 1997, A&AS, 124, 299
Cayrel de Strobel, G., Soubiran, C., & Ralite, N. 2001, A&A, 373, 159
Cincunegui, C., & Mauas, P. J. D. 2004, A&A, 414, 699
Cincunegui, C., Díaz, R. F., & Mauas, P. J. D. 2007, A&A, 461, 1107
Cox, A. N. 2000, Allen's astrophysical quantities (Allen's astrophysical quantities, 4th edn., ed. A. N. Cox (New York: AIP Press; Springer)
Duncan, D. K., Vaughan, A. H., Wilson, O. C., et al. 1991, ApJS, 76, 383
Giampapa, M. S., Cram, L. E., & Wild, W. J. 1989, ApJ, 345, 536
Glebocki, R., & Stawikowski, A. 2000, Acta Astron., 50, 509
Hall, J. C. 1996, PASP, 108, 313
Hall, J. C., Lockwood, G. W., & Gibb, E. L. 1995, ApJ, 442, 778
Henry, T. J., Soderblom, D. R., Donahue, R. A., & Baliunas, S. L. 1996, AJ, 111, 439
Hooten, J. T., & Hall, D. S. 1990, ApJS, 74, 225
Jenkins, L. F. 1952, General catalogue of trigonometric stellar parallaxes. ([New Haven, Yale University Observatory] 1952.)
Johnson, H. L. 1966, ARA&A, 4, 193
Labonte, B. J. 1986, ApJS, 62, 241
Linsky, J. L., McClintock, W., Robertson, R. M., & Worden, S. P. 1979, ApJS, 41, 47
Mauas, P. J. D., & Falchi, A. 1994, A&A, 281, 129
Mauas, P. J. D., Falchi, A., Pasquini, L., & Pallavicini, R. 1997, A&A, 326, 249
Middelkoop, F. 1982, A&A, 107, 31
Montes, D., Fernandez-Figueroa, M. J., de Castro, E., & Cornide, M. 1995, A&A, 294, 165
Noyes, R. W., Hartmann, L. W., Baliunas, S. L., Duncan, D. K., & Vaughan, A. H. 1984, ApJ, 279, 763
Pasquini, L., & Pallavicini, R. 1991, A&A, 251, 199
Pasquini, L., Pallavicini, R., & Pakull, M. 1988, A&A, 191, 253
Pasquini, L., Pallavicini, R., & Dravins, D. 1989, A&A, 213, 261
Perryman, M. A. C., Lindegren, L., Kovalevsky, J., et al. 1997, A&A, 323, L49
Pettersen, B. R. 1989, A&A, 209, 279
Reiners, A., & Schmitt, J. H. M. M. 2003, A&A, 398, 647
Robinson, R. D., Cram, L. E., & Giampapa, M. S. 1990, ApJS, 74, 891
Rutten, R. G. M. 1984, A&A, 130, 353
Saar, S. H., & Osten, R. A. 1997, MNRAS, 284, 803
Saar, S. H., Nordstrom, B., & Andersen, J. 1990, A&A, 235, 291
Ségransan, D., Kervella, P., Forveille, T., & Queloz, D. 2003, A&A, 397, L5
Soderblom, D. R., Stauffer, J. R., Hudon, J. D., & Jones, B. F. 1993, ApJS, 85, 315
Strassmeier, K. G., Fekel, F. C., Bopp, B. W., Dempsey, R. C., & Henry, G. W. 1990, ApJS, 72, 191
Thatcher, J. D., & Robinson, R. D. 1993, MNRAS, 262, 1
Vaughan, A. H., Preston, G. W., & Wilson, O. C. 1978, PASP, 90, 267
Wright, J. T., Marcy, G. W., Butler, R. P., & Vogt, S. S. 2004, ApJS, 152, 261

Online Material

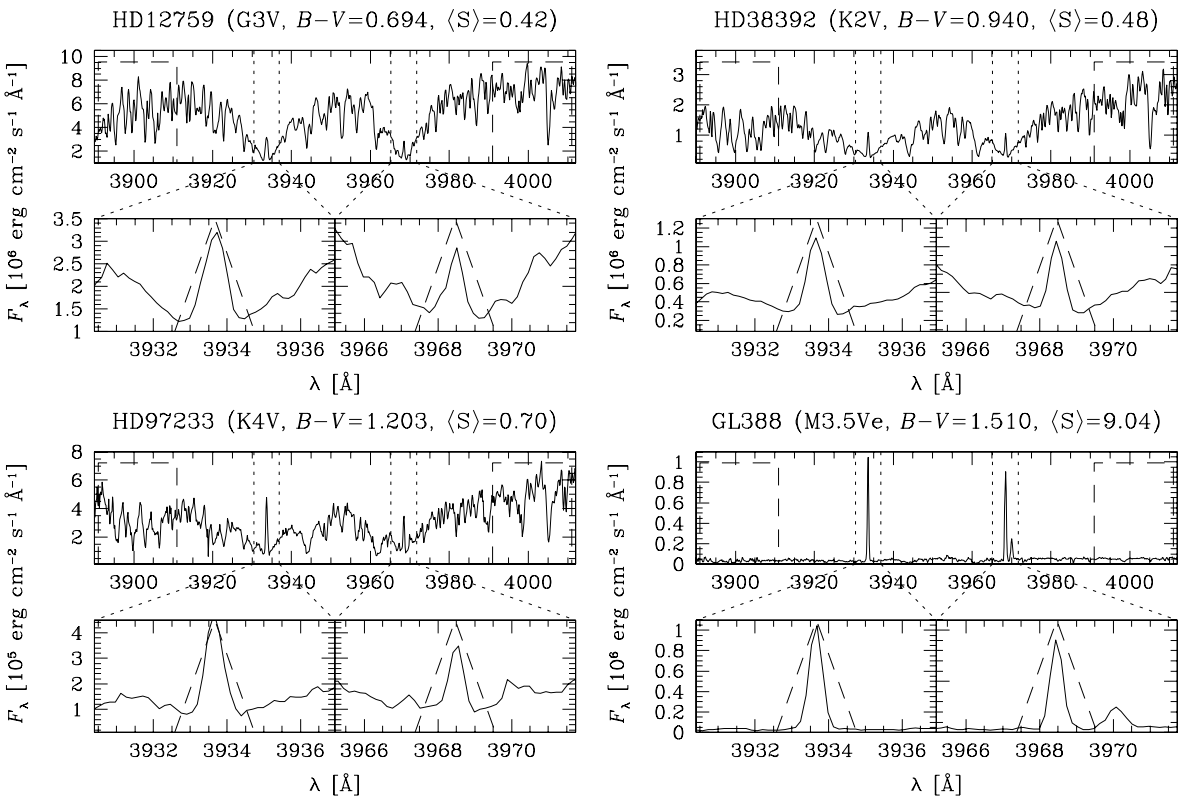

Fig. 1. Continued. Windows used to compute our S' index, for six stars of different spectral types and activity levels. For each star, we show in the top panel the whole spectral range used, with the continuum windows indicated with dashed lines. Below each of these spectra, we show in detail the H and K lines, and the triangular shape used to integrate the fluxes.

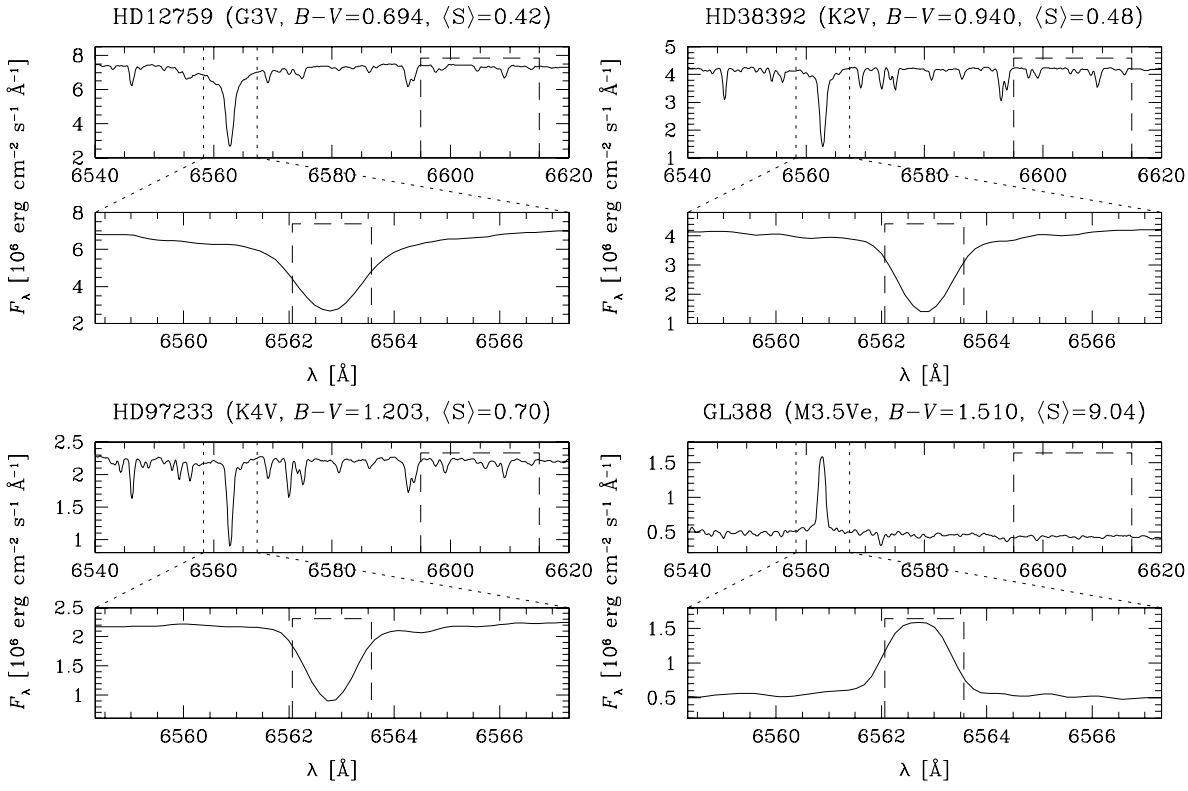

Fig. 6. Continued. Windows used to measure the fluxes in Hα, for six stars of different spectral types and activity levels, the same as in Fig. 1. For each star, we show in the top panel the whole range used, with the continuum window indicated with dashed lines. Below each of these spectra, we show in detail the Hα line, superimposed on the filter used to integrate the fluxes.

Table 1. Stars used to calibrate our S' index with the Mount Wilson S, as shown in Fig. 4. N is the number of spectra available for each star.

star	$B-V$	S	σ_S	N	S'	$\sigma_{S'}$
HD 38393	0.481	0.151	0.003	13	0.126	0.004
HD 16673	0.524	0.215	0.009	10	0.174	0.006
HD 45067	0.564	0.141	0.002	11	0.112	0.003
HD 30495	0.632	0.297	0.016	12	0.239	0.007
HD 9562	0.639	0.137	0.003	9	0.109	0.004
HD 11131	0.654	0.336	0.013	10	0.265	0.008
HD 1835	0.659	0.347	0.021	14	0.273	0.007
HD 158614	0.715	0.158	0.003	12	0.127	0.004
HD 3443	0.715	0.182	0.007	10	0.139	0.004
HD 3795	0.718	0.156	0.004	10	0.119	0.004
HD 10700	0.727	0.171	0.003	12	0.140	0.004
HD 152391	0.749	0.387	0.030	12	0.324	0.009
HD 219834	0.787	0.154	0.006	12	0.128	0.004
HD 26965	0.820	0.206	0.019	10	0.148	0.005
HD 17925	0.862	0.648	0.046	8	0.517	0.018
HD 22049	0.881	0.492	0.036	14	0.373	0.010
HD 23249	0.915	0.137	0.003	14	0.105	0.003
HD 38392	0.940	0.531	0.040	12	0.376	0.011

Table 2. Notes on the stars:
§: stars reported in CTIO as non-variable, which were used to calibrate the S indexes,
⋆: stars with planets,
◃: dMe stars, or stars presumably active,
†: RS CVn type,
‡: BY Dra type.
The spectral types, V magnitudes and $B-V$ colours are from Perryman et al. (1997), except the stars indicated with an [a] which are from Simbad database.
The parallexes are from Perryman et al. (1997), except the ones marked with a [b] that are from Jenkins (1952).
The gravity and metallicity are from Cayrel de Strobel et al. (2001), except the ones indicated with a [c] which are from Cayrel de Strobel et al. (1997).
The rotational periods are from: [d] Saar & Osten (1997), [e] Baliunas et al. (1996), [f] Noyes et al. (1984), [g] Saar et al. (1990), [h] Hooten & Hall (1990) and [i] Pettersen (1989). Also, we estimated periods from $v \sin i$ using [(j)] Glebocki & Stawikowski (2000) and [(k)] Reiners & Schmitt (2003).
The last two columns include the slope of the linear regression between $F_{H\alpha}$ and F_{HK} for the individual spectra of each star (m, see Fig. 11) and the corresponding correlation coefficient (ρ). The $F_{H\alpha}$ between parentheses were excluded from our analysis in Section 4.1, since they might be subject to larger errors due to the use of $B-V$ as a proxy for T_{eff} for stars with $B-V \leq 1.4$.

HD	GJ/GL	Name		Spectral type	V	$B-V$	Parall.	$\log g$	[Fe/H]	P_{rot}	N	$\langle S \rangle$	$\langle F_{HK} \rangle$ 10^4 erg cm^{-2} s^{-1}	$\langle F_{H\alpha} \rangle$ 10^5 erg cm^{-2} s^{-1} Å^{-1}	m	ρ
1835	17.3	BE Cet	§ ‡	G3V	6.390	0.659	49.05	4.22	−0.01	7.78 [d]	14	0.35	187.20	33.75	0.28	0.32
3405	24A			G0/G1V	6.790	0.639	22.79				5	0.33	219.10	46.33	−3.13	−0.88
3443	25A		§	K1V+...	5.570	0.715	64.38	4.57	−0.16 [c]	30.00 [e]	10	0.17	82.95	29.09	0.76	0.60
3795	27.2		§	G3/G5V	6.140	0.718	35.02	3.75	−0.70	32.00 [e]	10	0.15	70.85	28.05	0.31	0.38
4308	31.5			G3V	6.550	0.655	45.76	4.29	−0.47		13	0.16	94.45	30.47	0.04	0.18
4967	40			K5V	8.950	1.290	65.81				1	1.49	33.55	10.66		
5869				K4V	7.510	1.473	4.76				3	0.18	1.11	(31.14)	0.03	0.22
9562			§	G2IV	5.750	0.639	33.71	3.90	0.18	29.00 [e]	9	0.14	84.80	30.39	0.02	0.12
10700	71	tau Cet	§	G8V	3.490	0.727	274.17	4.30	−0.59	34.50 [d]	12	0.18	78.55	28.10	−0.02	−0.53
11131		chi Cet B	§	G0	6.720	0.654	43.47	4.50	−0.06	<5.21 [(j)]	10	0.33	213.10	36.16	0.11	0.41
12759				G3V	7.300	0.694	20.34				5	0.42	208.25	35.53	−0.50	−0.52
13445			⋆	K0V	6.120	0.812	91.63	4.75	−0.21	30.00 [d]	6	0.26	69.80	26.86	0.02	0.16
16673	3175		§	F6V	5.790	0.524	46.42	4.16	−0.01	7.00 [e]	10	0.22	225.85	38.10	0.21	0.30
17051		iot Hor	⋆	G3IV	5.400	0.561	58.00	4.22	−0.04	7.90 [d]	6	0.23	193.10	37.36	1.00	0.55
17576				G0V	7.830	0.609	6.13				5	0.84	614.00	54.48	−1.20	−0.95
17925	117	EP Eri	§ †	K1V	6.050	0.862	96.33	4.60	0.10	6.76 [d]	8	0.65	140.00	31.17	−0.14	−0.22
19034	121.2			G5	8.080	0.677	28.33				9	0.18	93.70	30.70	−0.06	−0.20
19467	3200			G3V	6.970	0.645	31.76				11	0.15	88.15	30.57	0.17	0.28
19994		94 Cet	⋆	F8V	5.070	0.575	44.69	4.10	0.15	8.59 [(j)]	10	0.17	138.25	33.27	1.94	0.78
20619	135			G0	7.050	0.655	40.52	4.48	−0.20		12	0.18	105.40	29.49	0.19	0.39
20766	136	zet01 Ret		G2V	5.530	0.641	82.51	4.54	−0.22	<12.10 [(k)]	13	0.25	157.45	33.10	0.15	0.31
22049	144	eps Eri	§ ‡	K2V	3.720	0.881	310.75	4.38	−0.14	11.68 [d]	14	0.47	89.90	24.74	0.12	0.42
23249	150	del Eri	§ ‡	K0IV	3.520	0.915	110.58	3.95	0.05	71.00 [e]	14	0.13	22.68	19.26	0.07	0.53
25069				G9V	5.850	1.001	22.88				6	0.12	13.01	15.77	1.30	0.75
26965	166A	DY Eri	§	K1V	4.430	0.820	198.24	4.31	−0.25	37.10 [d]	10	0.19	51.55	26.41	−0.02	−0.15
27442		eps Ret	⋆	K2IV	4.440	1.078	54.84	3.30	0.22	54.96 [(k)]	10	0.13	10.34	12.42	0.01	0.36
28246				F6V	6.380	0.457	27.00				6	0.21	303.10	39.55	0.08	0.76
30495	177	58 Eri	§	G3V	5.490	0.632	75.10	4.30	−0.13	9.10 [d]	12	0.30	194.40	33.28	0.22	0.47
32147				K3V	6.220	1.049	113.46	4.57	0.34	47.40 [d]	11	0.30	24.55	16.19	0.15	0.68
35850				F7V:	6.300	0.553	37.26	4.40	0.00	0.91 [(j)]	6	0.50	482.30	56.47	0.24	0.68
36395	205			M1V	7.970	1.474	175.72	4.80	0.60 [c]	<7.85 [(j)]	9	2.44	20.12	(6.70)	0.33	0.97
36435				G5V	6.990	0.755	51.10	4.49	−0.02	11.20 [d]	5	0.44	149.40	28.75	0.04	0.24
37572		UY Pic		K0V	7.950	0.845	41.90				12	0.79	211.05	36.38	0.14	0.34
38392	216B	gam Lep B	§	K2V	6.150	0.940 [a]		4.50	0.02	17.30 [d]	12	0.48	62.95	22.14	0.08	0.29
38393	216A	gam Lep	§	F7V	3.590	0.481	111.49	4.10	−0.12	13.22 [(j)]	13	0.16	188.15	39.16	0.04	0.06
38858	1085			G4V	5.970	0.639	64.25				6	0.16	102.85	32.39	0.16	0.34
39917		SZ Pic	†	G8V	7.890	0.813	5.13			4.48 [(j)]	10	0.54	158.10	47.64	−0.59	−0.57
41824			†	G6V	6.600	0.712	33.64				12	0.57	260.30	44.30	0.43	0.86
42581	229A		◃	M1/M2V	8.150	1.487	173.19			7.74 [(j)]	9	1.66	9.72	(4.73)	0.15	0.61
43587	231.1A			G0.5Vb	5.700	0.610	51.76		−0.08	20.00 [e]	8	0.15	100.40	32.81	−0.13	−0.65
45067			§	F8V	5.880	0.564	30.22	4.17	−0.16	8.00 [e]	11	0.14	125.20	32.46	0.05	0.27
45270				G1V	6.530	0.614	42.56				6	0.39	268.25	38.43	0.45	0.70
48189	3400A			G1/G2V	6.150	0.624	46.15				7	0.44	274.35	45.52	0.57	0.62
52265			⋆	G0III−IV	6.290	0.572	35.63	4.29	0.21	9.42 [(j)]	3	0.16	130.10	36.05	2.24	1.00
54579		V361 Pup		G0V	8.030	0.606	16.95				3	0.47	337.30	59.99	0.30	0.87
59967	3446			G3V	6.660	0.641	45.93			10.26 [(j)]	5	0.38	232.15	36.44	0.18	0.38
75289			⋆	G0Ia0:	6.350	0.578	34.55	4.51	0.28		8	0.15	118.45	33.25	0.05	0.84
82106	349		◃	K3V	7.200	1.002	78.87			13.30 [d]	15	0.32	32.57	17.93	0.18	0.45
94683				K4III	5.950	1.736	1.96				7	0.37	0.10	(0.26)	−0.36	−0.69
97233	416			K4V	9.060	1.203	44.00			7.60 [f]	10	0.70	21.62	13.71	−0.00	−0.00
101581	435		◃	K5V	7.770	1.064	79.91				9	0.49	29.16	17.98	0.06	0.41
103112	3689A			K0	7.610	1.055	12.39				9	0.15	13.17	14.55	−0.01	−0.24

Table 2. Continued.

HD	GJ/GL	Name		Spectral type	V	$B-V$	Parall.	log g	[Fe/H]	$P_{\rm rot}$	N	$\langle S \rangle$	$\langle F_{\rm HK} \rangle$ 10^4 erg cm^{-2} s^{-1} Å^{-1}	$\langle F_{\rm H\alpha} \rangle$ 10^5 erg cm^{-2} s^{-1} Å^{-1}	m	ρ
105115				K2/K3V	6.910	1.391	2.85				5	0.15	1.49	3.77	0.03	0.76
114762			⋆	F9V	7.300	0.525	24.65	4.10	−0.82	52.16 [j]	3	0.16	145.95	39.76		
117176		70 Vir	⋆	G5V	4.970	0.714	55.22	3.83	−0.11		4	0.10	38.85	28.15	−0.00	−0.06
118100	517	EQ Vir	◃	K7V	9.240	1.210	50.54	4.50	−0.15 [c]	3.90 [d]	9	3.68	118.55	25.63	0.75	0.98
119285		V851 Cen	†	K1Vp	7.640	1.068	13.13			12.03 [g]	5	0.51	34.76	21.57	0.39	1.00
119850	526		◃	M3V	8.460	1.435	184.13			8.60 [j]	9	0.57	5.45	(5.81)	0.40	0.53
120136		tau Boo	⋆	F7V	4.500	0.508	64.12	4.18	0.32	4.00 [e]	3	0.19	203.95	36.65	−0.14	−0.20
122303	536			K5	9.710	1.461	98.26				8	0.97	8.11	(6.99)	−0.04	−0.05
123732		V759 Cen		G0V	7.540	0.594	15.88				2	0.44	334.85	62.73	0.56	
125072	542			K3V	6.660	1.017	84.50	4.50	0.26		10	0.27	20.42	17.49	−0.09	−0.42
128620	599A	alf Cen A		G2V	−0.010	0.710	742.12	4.31	0.22	29.00 [d]	7	0.15	71.60	27.31	0.00	0.02
128621		alf Cen B		K1V	1.350	0.900	742.12	4.51	0.24	42.00 [d]	9	0.20	35.56	21.55	0.30	0.85
130948				G2V	5.860	0.576	55.73	4.18	−0.20	6.40 [j]	6	0.30	205.70	37.34	−0.00	−0.02
131977				K4V	5.720	1.024	169.32	4.58	0.03	44.60 [d]	9	0.51	33.00	19.37	0.01	0.11
144253	610			K3/K4V	7.390	1.043	53.93		−0.03		10	0.24	19.72	19.38	−0.21	−0.44
146233	616	18 Sco		G1V	5.490	0.652	71.30	4.49	0.05	23.70 [d]	15	0.17	95.00	31.49	0.03	0.06
147513	620.1A			G3/G5V	5.370	0.625	77.69	4.52	0.03	8.50 [d]	11	0.32	193.30	34.96	0.15	0.54
150433	634.1			G0	7.210	0.631	33.84				8	0.17	104.85	34.12	0.17	0.97
151770				G3/G5V	8.340	0.676	7.45				4	0.62	313.40	61.08	−0.64	−0.97
152391	641	V2292 Oph	§ ‡	G8V	6.650	0.749	59.04			11.43 [d]	12	0.41	147.10	32.02	0.03	0.17
156026	664	36 Oph C	†	K5V	6.330	1.144	167.56	4.67	−0.21	18.50 [d]	7	0.76	29.45	15.07	−0.06	−0.40
156425				K4V:	7.810	1.098			−0.20		7	0.41	5.79	13.33	0.02	0.06
157881	673			K7V	7.540	1.359	129.54	4.70	−0.20	7.29 [j]	10	0.78	8.44	8.12	0.05	0.71
158614	678A		§	G8IV−V	5.310	0.715	60.80	4.04	−0.05	34.00 [e]	12	0.22	66.25	27.97	−0.10	−0.58
160691	691	mu Ara		G5V	5.120	0.694	65.46	4.20	0.20	14.04 [k]	8	0.14	63.50	28.82	−0.00	−0.02
165185				G3V	5.940	0.615	57.58	4.49	−0.06	5.90 [d]	10	0.30	197.75	36.55	0.23	0.91
172051				G5V	5.850	0.673	77.02				13	0.17	92.60	31.32	−0.17	−0.42
173560	725.3			G3V	8.690	0.649	11.65				11	0.19	109.75	33.41	0.03	0.87
177996	4096			K1V	7.890	0.862	31.48				9	0.64	133.05	34.16	0.01	0.03
180617	752A		◃	M3.5V	9.120	1.464	170.26			16.80 [j]	8	1.08	10.03	(7.80)	0.04	0.20
187923	4126			G0V	6.160	0.642	36.15	3.97	−0.20	<3.72 [j]	10	0.14	85.00	35.15	0.02	0.20
188088	770	V4200 Sgr	‡	K3/K4V	6.220	1.017	70.34			16.50 [h]	6	0.59	56.35	19.15	−0.46	−0.58
189567	776			G2V	6.070	0.648	56.45	4.10	−0.30		8	0.17	94.00	32.60	0.02	0.28
197076	797A			G5V	6.430	0.611	47.65			13.21 [j]	7	0.16	90.60	34.66	−0.04	−0.15
197214	4157			G3/G5V	6.950	0.671	44.57				12	0.19	108.05	30.37	−0.00	−0.04
202628	825.2			G5V	6.750	0.637	42.04	4.52	−0.14		10	0.24	158.00	32.41	−0.01	−0.05
202917				G5V	8.650	0.690	21.81				6	0.68	358.35	51.16	0.34	0.66
202996				G0V	7.460	0.614	18.76				2	0.26	203.65	38.26	0.42	
203019				G5V	7.840	0.687	27.49				4	0.49	253.25	34.40	0.09	0.89
203244				G5V	6.980	0.723	48.86	4.49	−0.21		1	0.40	183.30	33.63		
209100	845	eps Ind	◃	K5V	4.690	1.056	275.76	4.50	−0.23	22.00 [d]	11	0.44	31.67	16.02	−0.14	−0.51
210918	851.2			G5V	6.230	0.648	45.19	4.43	−0.18		12	0.16	96.35	29.92	0.03	0.10
212330	857			F9V	5.310	0.665	48.81	4.00	−0.04	<21.05 [j]	10	0.14	72.75	29.99	0.01	0.07
213240			⋆	G4IV	6.810	0.603	24.54				3	0.18	132.65	33.91	0.09	0.96
213941	863.3			G5V	7.580	0.670	30.98		−0.42		9	0.19	124.10	29.15	−0.16	−0.41
215768				G0V	7.490	0.589	25.34				5	0.31	233.15	37.36	0.17	0.32
216803		TW PsA		K4Vp	6.480	1.094	130.94			10.30 [d]	3	1.00	61.20	18.68	−0.75	−0.93
217343				G3V	7.470	0.655	31.22				2	0.47	285.55	36.22	−0.03	
219709				G2V	7.500	0.632	25.33		−0.02		8	0.22	147.80	31.15	0.08	0.24
219834	894.2A	94 Aqr	§	G6/G8IV	5.200	0.787	48.22 [b]	3.90	0.09	42.50 [e]	12	0.16	53.55	24.71	−0.22	−0.51
225213	1			M2V	8.560	1.462	229.33				10	0.36	3.06	(7.53)	0.03	0.10
	375	LU Vel	◃	M5	11.270	1.555	62.88				14	2.56	6.33	(4.74)	0.34	0.46
	388	AD Leo	◃	M3.5Ve	9.430	1.540 [a]	213.00 [b]			2.60 [i]	7	9.04	30.89	(13.15)	0.15	0.38
	479			M3	10.650	1.470	103.54				7	1.78	13.32	(10.16)	0.07	0.41
	551	Proxima Cen	◃	M5Ve	11.010	1.807	772.33				22	4.10	1.68	(2.05)	0.10	0.31
	699	Barnard's star	◃	sdM4	9.540	1.570	549.01			2.09 [j]	11	0.93	2.61	(2.48)	0.04	0.20
	729	V1216 Sgr	◃	M3.5Ve	10.370	1.510	336.48				1	6.98	79.85	(30.12)		